J Mater Sci (2012) 47:4282–4289
DOI 10.1007/s10853-012-6278-5

Temperature-dependence on the optical properties and the phase separation of polymer–fullerene thin films

Gerald F. Malgas · David E. Motaung · Christopher J. Arendse

Received: 20 October 2011 / Accepted: 16 January 2012 / Published online: 26 January 2012

Abstract A detailed study on the thermal transition of poly(3-hexylthiophene) (P3HT) and blends was investigated by differential scanning calorimetry, while the morphological, phase separation and the transformation in the optical properties were probed by thermal-atomic force microscopy (AFM), polarized optical microscopy (POM) and spectroscopic ellipsometry (SE). The inclusion of fullerenes on the polymer structure confirms the formation and evolution of a new endothermic transition at high temperatures. SE revealed that the refractive index and extinction coefficient of the films increased with annealing temperature up to 140 °C due to the suppressed diffusion of PCBM molecules into the blend. Annealing above 140 °C resulted in a decrease in the optical constants due to the formation of large "needle-like" crystals. This is due to the depletion of PCBM clusters near the "needle-like" structures; resulting from the diffusion of the PCBM molecules into the growing PCBM crystals or "needle-like" crystals as is evidenced by in situ thermal-AFM and POM. These findings indicate that annealing temperature of 140 °C is suitable for a P3HT:PCBM film to obtain the desired phase separation for solar cell application.

G. F. Malgas (✉) · D. E. Motaung (✉)
DST/CSIR Nanotechnology Innovation Centre, National Centre for Nano-structured Materials, Council for Scientific Industrial Research, P. O. Box 395, Pretoria 0001, South Africa
e-mail: gmalgas@csir.co.za

D. E. Motaung
e-mail: dmotaung@csir.co.za

C. J. Arendse
Department of Physics, University of the Western Cape, Private Bag X17, Bellville 7535, South Africa

Introduction

Due to the demand of inexpensive clean energy, renewable energy problems have considerable attention in the past several decades [1–5]. Conjugated polymers have great potential for cost effectiveness and a wide field of applications in photovoltaic devices due to their mechanical flexibility and low weight of polymer materials [2, 6–8]. The easy thin film fabrication technology based on solution process such as spin coating, doctor blade and printing could lead to a reduction of the production costs of large-area solar cells [9, 10]. In addition, the band gap of the polymer can be easily varied and thus absorb light at different wavelengths due to the flexibility of organic synthesis and chemical tailoring [11].

The most successful organic photovoltaic active material system consists of a bulk heterojunction (BHJ) that is formed by a p-type semiconductor (electron donor), such as poly(3-hexylthiophene) (P3HT) with an n-type semiconductor (electron acceptor), such as methanofullerene derivatives (PCBM). However, for all these advantages associated with this novel technology, power conversion efficiency of polymer solar cells is still relatively low compared to inorganic solar cells. To improve the efficiency of solar cells, parameters such as the structure of the polymer, the morphology of the film, the interfaces [12] between the layers (organic/metal, organic/organic), and the choice of electron acceptor and the ratio between this and the polymer [13] and the choice of solvent still need to be understood. Previous results showed that a limited solubility of P3HT and C_{60} fullerene in a marginal solvent such as non-aromatic solvent can lead directly to optimal morphologies on the films [14]. Researchers proposed different experimental methods for the optimization of the morphology, such as thermal annealing [15–19], solvent

annealing [20, 21] and substrate annealing [22] or the use of additives [23, 24] that can lead to a molecular rearrangement of the spin-coated film. Solvent annealing (either slow evaporation of the solvent or exposure to solvent vapour even after the films have dried), and thermal annealing have been successfully used to increase the device performance by PCBM diffusion and P3HT crystallization. These processes significantly increase the polymer's hole mobility and absorption [25–28]. Although P3HT:PCBM properties have been extensively studied, not much work has been done to understand the surface morphology changes of P3HT:PCBM in situ by varying the temperature. Therefore, in this article we investigate the thermal behaviour of P3HT and blended films and the changes on the surface morphology using atomic force microscopy (AFM) equipped with a heating apparatus (thermal-AFM) and polarized optical microscopy (POM) (also equipped with heating stage) to study the phase separation in the nanoscale morphology in situ at the nanoscale. The AFM tip is employed to scan the specific area of the film upon heating and allows us to observe the changes on the surface at different temperatures. Spectroscopic ellipsometry (SE) and differential scanning calorimetry (DSC) was used to monitor the evolution of the optical constants during annealing and the degree of crystallinity of the materials, respectively.

Experiment details

Materials and thin film preparation

Silicon (Si) substrates were cleaned with organic solvents. Regioregular-P3HT polymer (molecular weight (M_w) of $\sim$64,000 g mol^{-1}; regularity >98.5%), C_{60} (purity of 99.5%), C_{60} derivative, PCBM (purity 99.5%) were purchased from Sigma Aldrich and used as received without any purification. Photoactive layers were prepared by mixing P3HT with C_{60} or PCBM in a 1:1 weight ratio and dissolving the constituents in a chloroform solution and stirred overnight at 50 °C. Films were prepared by spin coating the solution on top of the Si and followed by evaporation of the solvent at 50 °C.

Characterization

Differential scanning calorimetry

The melting and crystallization kinetics were studied by DSC measurements with a TA Q2000 instrument. Approximately 4.0 mg of each sample was loaded in a sealed aluminium pan. The analyses were conducted from −50 to 320 °C at a fixed heating rate of 15 °C min^{-1} and cooling rates of 5, 10 and 15 °C min^{-1} in a nitrogen flow rate of 5 mL min^{-1}. Isothermal crystallization was monitored after rapidly cooling samples from 320 °C to the desired temperature. For DSC measurements, the degree of crystallinity, X, of the P3HT and blended samples, was calculated according to:

$$X = \frac{\Delta H}{\Delta H_0} \quad (1)$$

where ΔH is the enthalpy of fusion determined by integrating DSC endotherms normalized to the respective weight fractions and ΔH_0 is the enthalpy of fusion of 100% crystalline material, with a ΔH_0 (P3HT) = 99 J g^{-1} [29, 30].

Polarized optical microscopy

Spin-coated thin films were placed between two covering glasses and placed on a Linkam hot-stage (Linkam Scientific Instruments Ltd, UK), mounted on a polarized optical microscope (POM) instrument. Films were heated from room temperature up to 250 °C at a heating rate of 10 °C min^{-1}, held at each temperature for 15 min and then cooled down to room temperature at a precisely controlled cooling rate of 10 °C min^{-1}.

Atomic force microscopy

The surface morphology evolution of the P3HT:PCBM film was measured by using AFM (Digital Instruments, Veeco NanoScope IV Multi-Mode) in a tapping mode. The AFM was equipped with thermal apparatus to study the morphology evolution during annealing in air. Thermal-AFM used an extra controller to apply heat to the sample. In thermal-AFM experiment, films were heated from 100 °C up to 160 °C with an increment of 10 °C min^{-1} and held at each temperature for 15 min.

Variable angle spectroscopic ellipsometry

The variable angle spectroscopic ellipsometry (VASE) spectra (Ψ) and (Δ) were obtained in the range of 250–1000 nm at room temperature by using a rotating-compensator instrument (J.A. Woollam, M-2000) at multi-angles of incidence (AOI) (65°, 70° and 75°). For clarity we show spectra only at 75° AOI since they behave similarly at different AOI. The films were regarded as a homogeneous material with film thickness modelled using either a Cauchy model [31]. The experimental data were fitted to obtain the optical functions of the blends using a Lorentz model. Model parameters were obtained by minimizing the error function which is defined by the following equation [32]:

$$\mathrm{MSE} = \frac{\sum \left[\frac{|\tan(\psi_{exp})-\tan(\psi_{cal})|}{\sigma_{\tan(\psi)}}\right]^2 + \left[\frac{|\cos(\Delta_{exp})-\cos(\Delta_{cal})|}{\sigma_{\cos(\Delta)}}\right]^2}{N-M-1} \quad (2)$$

where MSE is the mean square error, Ψ_{exp}, Δ_{exp} are the measured values and Ψ_{cal}, Δ_{cal} are the calculated values, N is the number of wavelengths at which measurements were performed and M is the number of parameters used in the fitting.

Results and discussion

Thermal analysis

DSC is one of the most important investigative tools to obtain information about the melting temperature, crystallization behaviour and the degree of crystallinity of the material. We used DSC to determine the melting temperatures of the polymer (P3HT), P3HT:C_{60} and P3HT:PCBM blended samples and the crystallinity. Figure 1 shows the melting behaviour of P3HT and P3HT blended with C_{60} and PCBM as well as the cooling cycles at different rates. The DSC traces of P3HT exhibits an exothermic transition from a crystalline to a liquid crystalline state at around 228.1 °C with a transition enthalpy (ΔH_f) of 17.8 J g^{-1} and glass transition (T_g) of about 49.1 °C as depicted in Fig. 1 and Table 1. The blended sample of P3HT and C_{60} shows both the crystal transition melting temperature associated with the fullerene component and the main-chain melting transition of the polythiophene [33].

However, the blended samples of P3HT with C_{60} and PCBM in Fig. 1 reveal a considerable shift in exothermic to lower temperatures (Table 1). The P3HT:PCBM blend

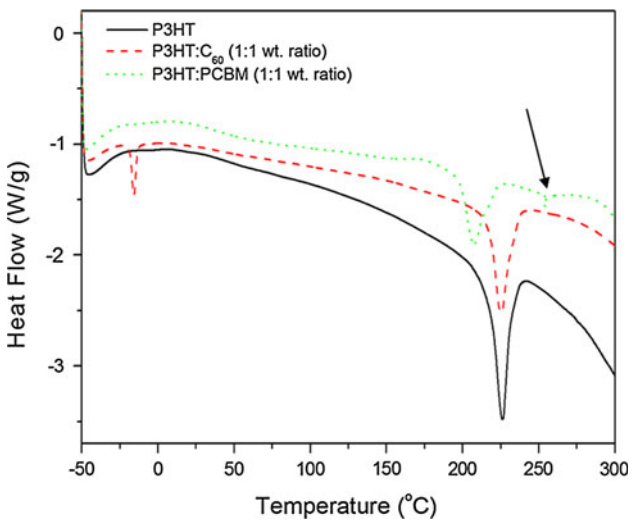

Fig. 1 Series of DSC profiles of P3HT and blend samples extracted at a heating rate of 15 °C min^{-1}

in Fig. 1a (arrows) displays two melting peaks at 207.4 and 217.7 °C ($\Delta H_f = 9.8$ J g^{-1} and $T_g = 48.0$). These thermal transitions are the fingerprints of the thermal behaviour of the polymer component, signifying that the semi-crystalline nature of P3HT is still persistent, being only moderately hindered by a fullerene.

It is also believed that the melting point depressions observed in both the blended films are expected because the fullerene acts as an impurity that depresses the freezing (melting) temperature of the semi-crystalline polymer [34]. The cooling run of P3HT of 5 °C min^{-1} shows an endothermic transition centred at 199.5 °C with enthalpy of 26.4 J g^{-1}; while the cooling successive scan of 15 °C min^{-1} displays an endothermic transition at 196.4 °C and enthalpy of 25.3 J g^{-1}, Fig. 2. In addition, alterations in polymer structure are also noticeable in the cooling curves and Table 2.

Morphological analysis

The phase separation and microstructure of the P3HT:PCBM film was characterized by in situ POM analysis to attain useful information on the effects of temperature treatment in the photoactive layer as depicted in Fig. 3. It is observed in Fig. 3a that the as-prepared film reveals a rather smooth surface. The phase contrast optical microscopy image in Fig. 3b of the annealed film at 140 °C shows the formation of "needle-like" shape crystals of PCBM with different density. It is interesting to note that upon increasing the temperatures to 160 °C, Fig. 3c, d, nanoscopic PCBM domains or clusters that are already present in both the lower regions of the spin-coated film and near the air surface move towards the needle-like shape structures, resulting into the formation of larger needles.

The surface morphology of the film changed completely after thermal heating at 230 °C, Fig. 3, showing a decrease in the sizes of the "needle-like" crystals or the needles. This is probably due to the melting of the PCBM resulting to the low density of the PCBM needles. The observed coloured 'halos' around the "needle-like" crystals are attributed to light interference originating from changes in film thickness and are due to PCBM-depleted regions. Motaung et al. [14] showed that a depletion of fullerene can also occur at low temperatures (72–170 °C). It is therefore vital to understand the mechanism related to the generation of functional structures in conjugated polymers. The nucleation of PCBM crystals is correlated with the temperature or energy, since the growth crystals require unobstructed space to expand. The surface energies of P3HT and PCBM are 26.9 and 38.2 mN m^{-1} [35, 36], respectively. At high temperatures (>150 °C) a large free volume is possible due to a randomly distributed polymer chains. Therefore at this temperature PCBM molecules

Table 1 Exothermical transition temperatures and the enthalpies per gram of P3HT and the blends (on the second DSC heating scan)

Samples	$T_{m\ (onset)}$ (°C)	$T_{m\ (finish)}$ (°C)	T_m (°C)	ΔH_f (J g^{-1})	Crystallinity (%)
P3HT	153.3	243.0	228.1	17.8	18.0
P3HT:C_{60}	185.2	244.7	230.5	9.2	9.3
P3HT:PCBM	177.4	235.8	215.8	10.7	10.8

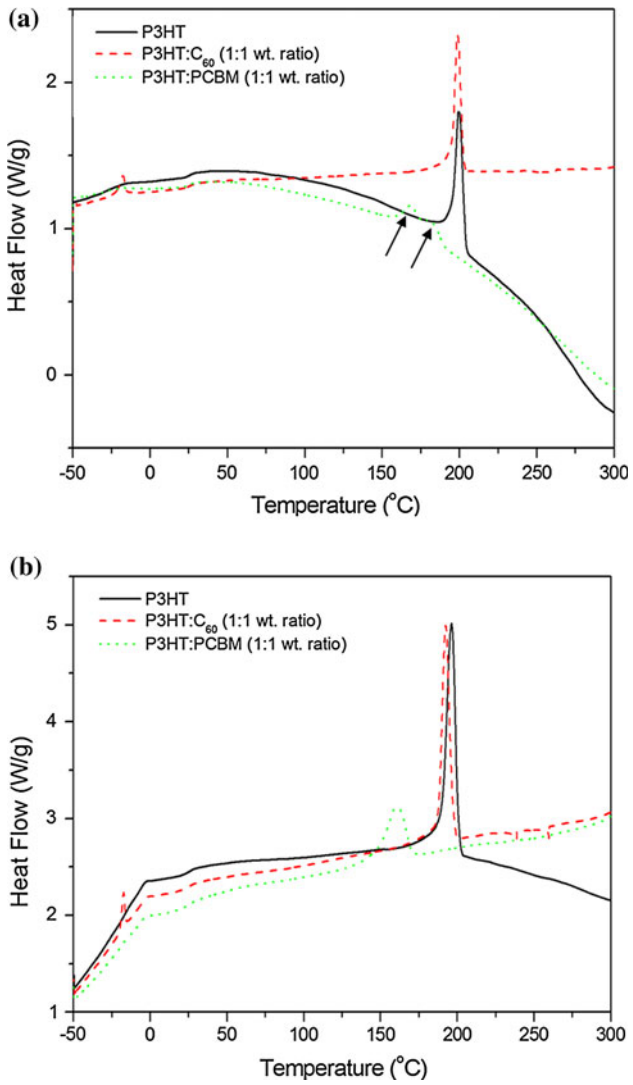

Fig. 2 Series of DSC profiles of P3HT and blended samples extracted at **a** cooling rate of 5 °C min^{-1} and **b** cooling rate of 15 °C min^{-1}

diffuse freely into the blended films and readily form large clusters which result to "needle-like" crystals. As the temperature increases, the formation and size of these needles increases due to the improved volume expansion induced by the soft chains of the polymer.

In order to complement the POM results, in situ AFM was employed to monitor the surface morphology changes of the P3HT:PCBM as shown in Fig. 4. It is interesting to note that upon heating the film at 140 °C, "needle-like" structures relating to PCBM crystals forms as depicted by arrows. Large needles appears as the temperature reaches 150 °C (results not shown), and the size and amount increases dramatically at 160 °C due to the soft P3HT chains that allow the PCBM particles to move easily. It seems reasonable to hypothesize that the increase in the "needle-like" crystals is due to the depletion of PCBM clusters near the "needle-like" structures; resulting from the diffusion of the PCBM molecules into the growing PCBM crystals or "needle-like" crystals, which create a localized sink as formerly conferred by Klimov et al. [37]. These "needle-like" crystals have diameter and length in the range of 1.2–2.0 μm and 10 μm, respectively.

To analyse the changes in the morphology quantitatively, the surface root mean square (rms) roughness values were measured as shown in Fig. 4f. A slight linear increase in the rms roughness is observed up to 140 °C for the blended film. Around the glass transition (T_g) of P3HT, the chains are soft and flexible and the surface of the blended film becomes flatter than that at lower temperature. At 160 °C, the PCBM particles are aggregated easily inside the soft P3HT thus resulting in a large extent to the phase separation. Thus, the roughness of the P3HT:PCBM film increases extensively, and further decline at 230 °C, Fig. 4f. Therefore, it can be concluded that the temperature 140 °C is suitable for a P3HT:PCBM film to obtain the desired phase separation for solar cell application.

Optical analysis

Figure 5 depicts the calculated pseudodielectric function (closed and open squares) spectra of P3HT and its blends extracted at different AOI, together with data of Ψ (solid lines) and Δ (solid lines). The fits show the excellent agreement between the model calculation and the experimental data, as confirmed by the MSE values in Table 3. For clarity we only show the 75° AOI spectra since they behave similarly at different AOI. The extracted optical constants of P3HT:PCBM film are depicted in Fig. 6. It is observed in Fig. 6a that the extinction coefficient of P3HT has two optical absorptions and a shoulder at 2.24, 2.45 and 2.05 eV. The first optical absorption at 2.24 eV is attributed to the formation of excitons with phonons [38] whereas the absorption peak at 2.45 corresponds to the 0–1

Table 2 Endothermical transition temperatures and the enthalpies per gram of P3HT and blends extracted at different cooling rates

Samples	Cooling rates (°C min^{-1})	$T_{c\ (onset)}$ (°C)	$T_{c\ (finish)}$ (°C)	T_c (°C)	ΔH_f (J g^{-1})	Crystallinity (%)
P3HT	5	221.8	155.4	206.0	24.2	24.4
P3HT	15	207.8	137.3	201.1	23.9	24.2
P3HT:C_{60}	5	211.5	154.3	202.6	11.2	11.3
P3HT:C_{60}	15	209.1	147.3	197.4	14.9	15.0
P3HT:PCBM	5	195.9	154.6	187.8	14.1	14.2
P3HT:PCBM	15	191.1	123.6	180.4	11.8	11.9

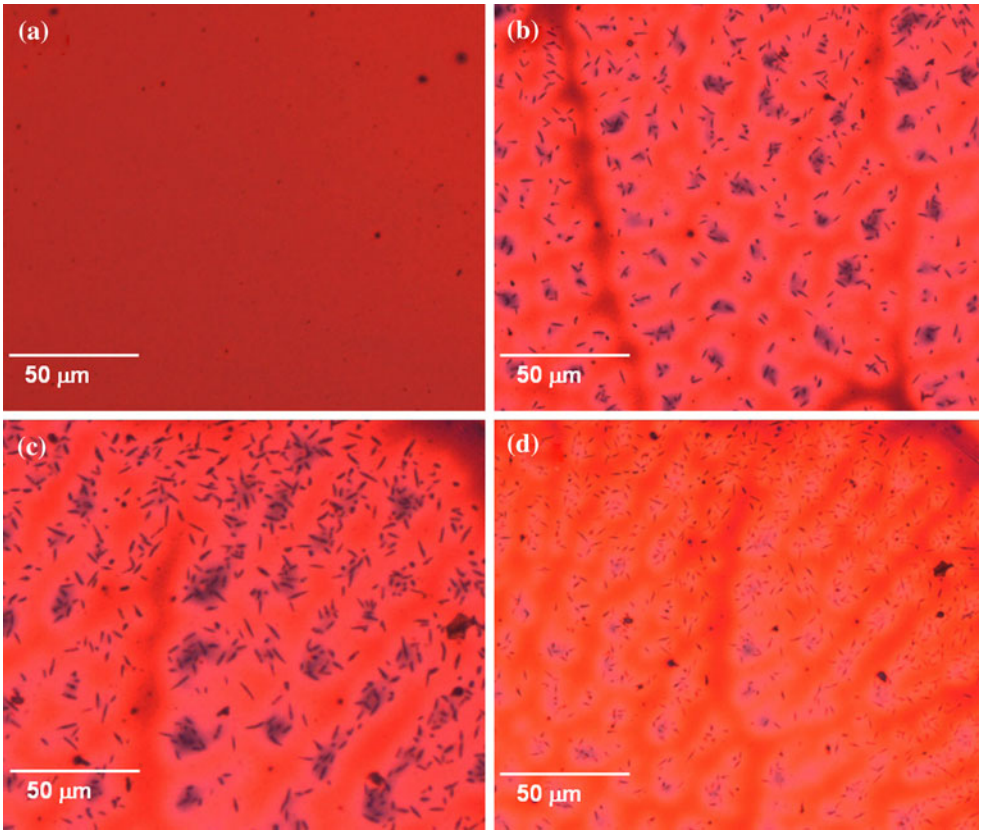

Fig. 3 In-situ polarized optical microscopy images of P3HT:PCBM film extracted at different temperatures: **a** as-prepared (RT), **b** 140 °C, **c** 160 °C and **d** 230 °C

transitions. The transition at 2.05 eV corresponds to the singlet excitonic transition of the P3HT conjugated polymer [39, 40]. The other two electronic transitions at 3.37 and 3.84 eV originate from the PCBM and are assigned to the electronic transitions $S_0 \rightarrow S_{17}$ and $S_0 \rightarrow S_{37}$, respectively [41]. It is evident from Fig. 6a that an enhancement in excitonic peak of the P3HT oscillator strengths is observed with annealing temperature up to 140 °C and degrades thereafter, until its melting point at 230 °C as shown by the DSC results.

This excitonic enhancement is related with the increase of the P3HT crystallization, which increases inter-chain interaction [28, 42]. As high density P3HT crystals start to form, pathways between the polymer crystallites are created, that facilitate the diffusion of PCBM molecules. Significant changes are observed in peaks relating to PCBM, the peaks reduce with annealing temperature. This indicates that the highly ordered P3HT crystals suppressed or retarded the diffusion of PCBM molecules into the blend and subsequently limited the enlarged growth of the PCBM needles as depicted in the AFM results. However, at higher temperatures, a broad absorption peak between 2.20 and 4.2 eV resulting from the formation of larger needle-shape crystals of PCBM and a possible melting of the P3HT is observed. Figure 6b shows that the refractive index abnormal dispersion curves are peaked at 1.05, 1.17 and

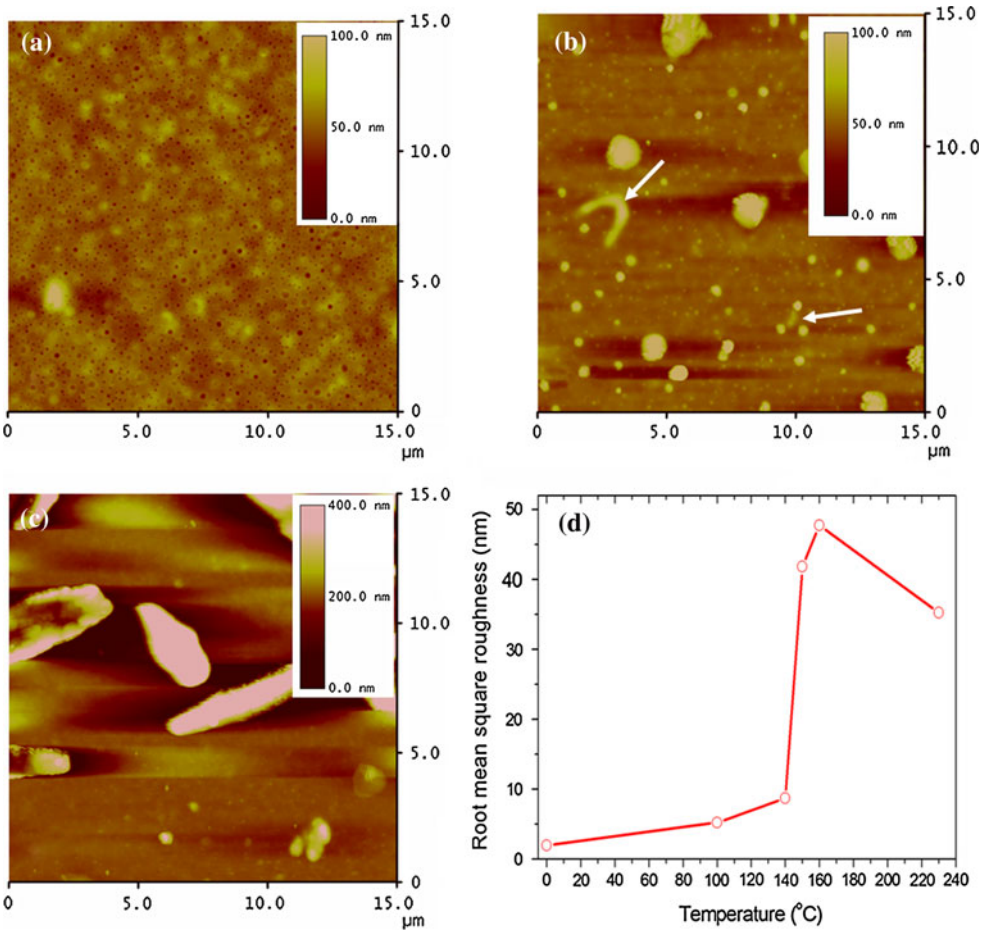

Fig. 4 AFM height (15 × 15 μm) images of P3HT:PCBM film of the **a** as-prepared and annealed at **b** 140 °C, **c** 160°C and **d** the corresponding root mean square roughness values of the P3HT:PCBM film as a function of temperature

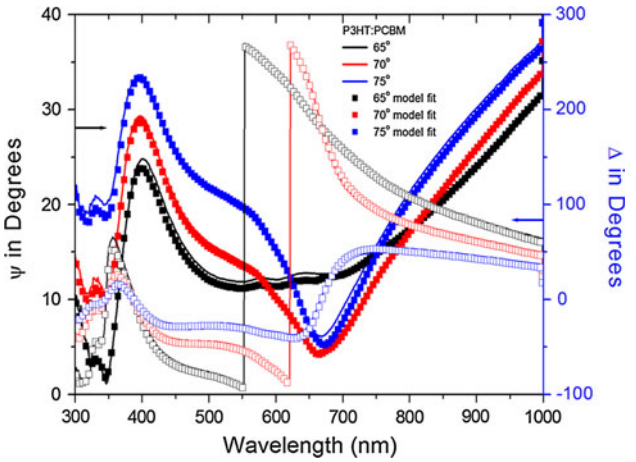

Fig. 5 Measured Ψ (*solid lines*) and Δ spectra (*solid lines*) with the model calculation (*closed and open squares*) for P3HT:PCBM film at different AOI

1.04 and for films annealed at 100, 140 and 150 °C, respectively, as compared with 1.02 of as-prepared film. The increased refractive index of annealed samples is due to the increased density from P3HT crystallization. However, the crystallization is disrupted with excessive annealing from 160 °C to the melting point of the polymer (230 °C), which results in a lower refractive index of 1.01 and 0.96 due to possible degradation of the polymer [27].

Conclusion

In summary, an inclusive study on the thermal transition of P3HT and blended films was investigated by means of DSC, thermal-AFM, POM and SE. The inclusion of the fullerenes on the polymer structure confirmed the formation and the evolution of a new endothermic transition occurring at higher temperature. SE demonstrated a reduction in the electronic peaks relating to PCBM, which resulted to the improved extinction coefficient and refractive index during annealing at 140 °C. This can be ascribed to the highly ordered P3HT crystals suppressing the diffusion of PCBM molecules into the blend and subsequently limited the enlarged growth of the "needle-like" structures. The results established that the annealing temperature of 140 °C is suitable for a P3HT:PCBM film to obtain the desired phase separation for solar cell application. These findings denote that the combination of the thermal-AFM

Table 3 Fitting errors at different temperatures using SE

Annealing temperature (°C)	MSE
As-prepared (RT)	41.55
100	54.27
140	38.05
150	43.54
160	46.91
180	47.11
200	41.63
230	52.88
250	60.84

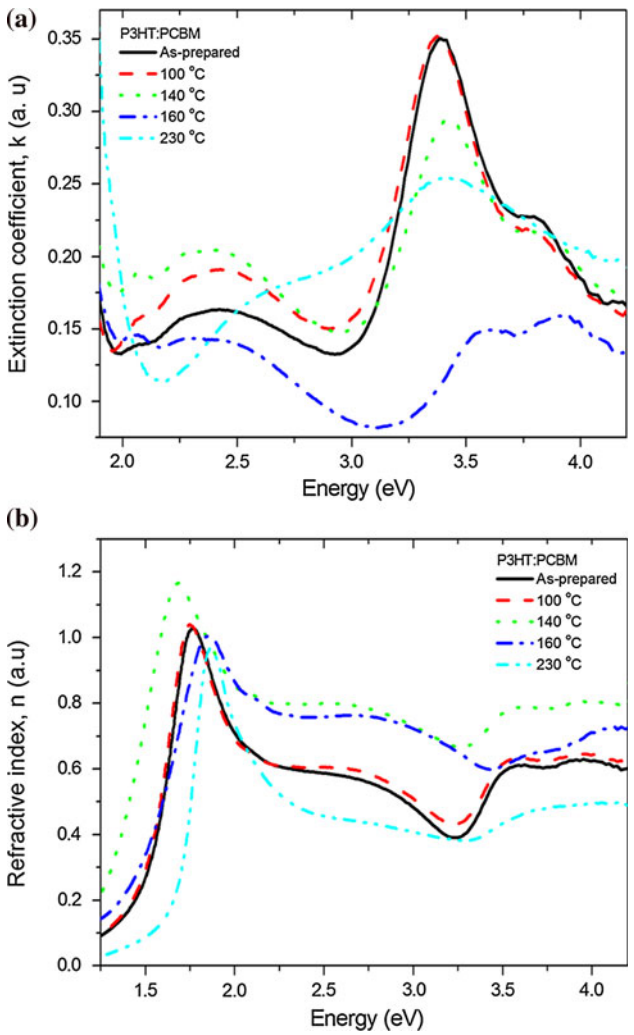

Fig. 6 Calculated **a** extinction coefficient (k) and **b** refractive index (n) as a function of energy for P3HT:PCBM annealed at different temperatures

and POM can open up the possibility of optimization of the morphology for the optimal absorption and phase separation for the solar cell efficiencies.

Acknowledgements The authors are grateful for the financial support of the Council for Scientific and Industrial Research and the Department of Science and Technology of South Africa.

References

1. Brabec CJ (2004) Sol Energy Mater Sol Cells 83:273
2. Brabec CJ, Sariciftci NS, Hummelen JC (2001) Adv Funct Mater 11:15
3. Brabec CJ, Cravino A, Meissner D, Sariciftci NS (2001) Adv Funct Mater 11:374
4. Shaheen S, Brabec CJ, Padinger F, Fromherz T, Hummelen JC, Sariciftci NS (2001) Appl Phys Lett 78:8414
5. Lee W, Shin S, Han S-H, Cho BW (2008) Appl Phys Lett 92:193307
6. Malgas GF, Arendse CJ, Mavundla SE, Cummings FR (2008) J Mater Sci 43:5599. doi:10.1007/s10853-008-2797-5
7. Lee W, Lee J, Lee S-H, Chang J, Yi W, Han S-H (2007) J Phys Chem C 111:9110
8. Lee W, Min S-K, Shin S, Han S-H, Lee S-H (2008) Appl Phys Lett 92:023507
9. Li G, Shrotriya V, Huang J, Yao Y, Moriarity T, Emery K, Yang Y (2005) Nat Mater 4:864
10. Brabec CJ, Padinger F, Hummelen JCR, Janssen AJ, Sariciftc NS (1999) Synth Met 102:861
11. Soci C, Hwang IW, Moses D, Zhu Z, Waller D, Gaudiana R, Brabec CJ, Heeger AJ (2007) Adv Funct Mater 13:632
12. Ishii H, Sugiyama K, Ito E, Seki K (1999) Adv Mater 11:605
13. Hoppe H, Sariciftci NS (2006) J Mater Chem 16:45
14. Motaung DE, Malgas GF, Arendse CJ (2010) Synth Met 160:876
15. Ma W, Yang C, Gong X, Lee K, Heeger AJ (2005) Adv Funct Mater 151:617
16. Padinger F, Rittberger RS, Sariciftci NS (2003) Adv Funct Mater 13:85
17. Motaung DE, Malgas GF, Arendse CJ, Mavundla SE, Oliphant CJ, Knoesen D (2009) J Mater Sci 44:3192. doi:10.1007/s10853-009-3425-8
18. Kim Y, Choulis SA, Nelson J, Bradley DDC, Cook S, Durrant JR (2005) J Mater Sci 40:1371. doi:10.1007/s10853-005-0568-0
19. Qiao F, Liu A, Hu Z, Liu Y, Yu S, Zhou Z (2009) J Mater Sci 44:3462. doi:10.1007/s10853-009-3461-4
20. Li G, Shrotriya V, Huang JS, Yao Y, Moriarty T, Emery K, Yang Y (2005) Nat Mater 4:864
21. Li G, Yao Y, Yang H, Shrotriya V, Yang G, Yang Y (2007) Adv Funct Mater 17:1636
22. Motaung DE, Malgas GF, Arendse CJ, Malwela T (2010) Mater Chem Phys 124:208
23. Lee JK, Wan L, Ma CJ, Brabec CJ, Yuen JS, Moon JY, Kim K, Lee GC, Bazan AJ, Heeger A (2008) J Am Chem Soc 130:3619
24. Chen L-M, Hong Z, Li G, Yang Y (2009) Adv Mater 21:1434
25. Mihailetchi VD, Xie H, de Boer B, Koster LJA, Blom PWM (2006) Adv Funct Mater 16:699
26. Cho S, Lee K, Yuen J, Wang G, Moses D, Heeger AJ, Surin M, Lazzaroni R (2006) J Appl Phys 100:114503
27. Motaung DE, Malgas GF, Arendse CJ (2011) J Mater Sci 46:4942. doi:10.1007/s10853-011-5408-9
28. Zhokhavets U, Erb T, Gobsch G, Al-Ibrahim M, Ambacher O (2006) Chem Phys Lett 418:347
29. Wunderlich B, Dole M (1957) J Polym Sci 24:201
30. Malik S, Nandi AK (2002) J Polym Sci Part B Polym Phys 40:2073
31. Woollam JA (2008) Inc. Complete Ease™ Data Analysis Manual, June 15
32. Jellison GE (1993) Thin Solid Films 234:416

33. Motaung DE, Malgas GF, Arendse CJ, Mavundla SE, Oliphant CJ, Knoesen D (2009) Sol Energy Mater Sol Cells 93:1674
34. Sperling LH (2001) Introduction to polymer science, 3rd edn. Wiley, Hoboken, NJ
35. Wang X, Ederth T, Inganäs O (2006) Langmuir 22:9287
36. Björström CM, Nilsson S, Bernasik A, Budkowski A, Andersson M, Magnusson KO, Moons E (2007) Appl Surf Sci 253:3906
37. Klimov E, Li W, Yang X, Hoffmann GG, Loos J (2006) Macromolecules 39:4493
38. Lioudakis E, Othonos A, Alexandrou I, Hayashi Y (2007) J Appl Phys 102:083104
39. Lioudakis E, Othonos A, Alexandrou I, Hayashi Y (2007) Appl Phys Lett 91:111117
40. Motaung DE, Malgas GF, Arendse CJ (2010) J Mater Sci 45:3276. doi:10.1007/s10853-010-4339-1
41. Harris DC, Bertolucci MD (1978) Symmetry and spectroscopy. Oxford University Press, New York
42. Campoy-Quiles M, Ferenczi T, Agostinelli T, Etchegoin PG, Kim Y, Anthopoulos TD, Stavrinou PN, Bradley DDC, Nelson J (2008) Nat Mater 7:158